International Journal of Greenhouse Gas Control 96 (2020) 103016

Contents lists available at ScienceDirect

International Journal of Greenhouse Gas Control

journal homepage: www.elsevier.com/locate/ijggc

Increased CO_2 storage capacity using CO_2-foam

T. Føyen[a,b,*], B. Brattekås[a], M.A. Fernø[a], A. Barrabino[b], T. Holt[b]

[a] Department of Physics and Technology University of Bergen, Norway
[b] SINTEF Industry, Norway

ARTICLE INFO

Keywords:
Carbon capture storage and utilization
CO_2 Storage Capacity
Decreased residual water saturations
Foam generation
Surfactant partitioning
Foam apparent viscosity
Non-ionic surfactants

ABSTRACT

Reduction of the CO_2 mobility is beneficial during subsurface sequestration of anthropogenic CO_2 in saline aquifers and hydrocarbon reservoirs by mitigating flow instabilities leading to early gas breakthrough and poor sweep efficiency. Injection of CO_2 foam is a field-proven technology for gas mobility control. Foam generation and coalescence are compared between six commercially available surfactants with a range in CO_2 solubility, during unsteady state injection of dense CO_2-foam in a long sandstone outcrop core (1.15 m). Foam generation categories and foam decay were defined based on the observed changes in foam apparent viscosity during generation and coalescence. The degree of CO_2 solubility influenced apparent viscosity development and peak foam strength for the tested surfactants. Variations in foam peak strength resulted in a range of water saturations at CO_2 breakthrough (up to 24 percentage points difference observed experimentally), with implications for the CO_2 storage capacity.

1. Introduction

Sequestration of anthropogenic CO_2 in subsurface geological formations is considered necessary in most scenarios to limit global warming to 1.5 °C (IPCC, 2018) and to meet the emission goals set forward by the Paris Agreement. For decades CO_2 has been pumped into geological formations containing hydrocarbons with the focus of enhancing the oil recovery (EOR) with variable degree of success (Lake et al., 2019), and without the focus of maximizing sequestered CO_2 in the formation. Co-optimizing CO_2 EOR, both in terms of oil produced and volumes of CO_2 stored, may act as a stepping-stone for large-scale sequestration of CO_2, because CO_2 EOR tackles the current largest obstacle to implementation; it represents an economic opportunity for the industry. The Carbon-Capture, Utilization and Storage (CCUS) value chain renders CO_2 sequestration cost efficient by establishing the necessary infrastructure and driving technology development (Ettehadtavakkol et al., 2014; Lindeberg et al., 2017).

The sweep efficiency during CO_2-EOR operations or aquifer CO_2 sequestration may be low. The low viscosity of CO_2 at reservoir conditions compared to the displaced brine and oil can cause viscous fingering, leading to early CO_2 breakthrough and high gas oil production ratios (Jones et al., 2016; Lee and Kam, 2013). Sweep efficiency challenges are further amplified in presence of reservoir heterogeneities, and result in low utilization of the injected CO_2 with lower-than-expected oil recovery, less CO_2 sequestered, and additional costs from the need to separate and recycling the produced gas. CO_2 mobility control is necessary to improve the sweep efficiency, and may be achieved using direct CO_2 thickeners (Cummings et al., 2012; Lee et al., 2014; Zhang et al., 2011) or CO_2 foam (Enick et al., 2012; Haugen et al., 2014; Vitoonkijvanich et al., 2015).

Foam can be described as discontinued gas phase, separated by a continuous thin liquid film called lamellae. Gas-flow resistance in each individual lamella is controlled by two different mechanisms: the drag associated with the viscous shear between a flowing/moving lamella (Hirasaki and Lawson, 1985), and the force needed to push a lamella through a pore throat (Falls et al., 1989). Foams are thermodynamically unstable systems and they require a stabilizer (foaming agent). The lamellae stabilization can be achieved by using surfactants or nanoparticles (Nguyen et al., 2014; Rognmo et al., 2017). Foam reduces the gas mobility more in high permeability zones relative to low permeability zones, and thus smoothen permeability contrasts (Bertin and Kovscek, 2003; Vassenden and Holt, 2000). When stable foam is present in high permeability zones fluids may be diverted into regions that have not previously been swept (Alcorn et al., 2019). The foaming agent

Abbreviations: CO_2, carbon dioxide; EOR, enhanced oil recovery; CCUS, carbon capture, utilization and storage; SAG, surfactant alternating gas; WASG, water alternating surfactant gas; SG, surfactant gas; BT, gas break through; PV, pore volume; AOS, Alpha olefin sulfonate; k, permeability; μapp, apparent viscosity; ∇p, pressure gradient; u, Darcy velocity; IFT, interfacial tension; kp, partition coefficient; Wt.%, weight percentage; $m_s^{x,t}$, mass of surfactant; $m_{CO_2}^{x-1,t-1}$, surfactant dissolved in CO_2; $m_{s,W}^{x,t-1}$, surfactant dissolved in Water; ρ_{CO_2}, CO_2 Density; S_W, water saturation

* Corresponding author at: Department of Physics and Technology University of Bergen, Norway.
E-mail address: tore.foyen@sintef.no (T. Føyen).

https://doi.org/10.1016/j.ijggc.2020.103016
Received 28 November 2019; Received in revised form 3 March 2020; Accepted 6 March 2020
Available online 11 March 2020
1750-5836/

must be selected for each specific case by evaluating factors such as the chemical stability at reservoir conditions, environmental concerns due to potential toxicity, economical aspects governed by price and volume of the foaming agent needed, in addition to the foaming agent ability to generate a sufficiently strong and stable foam.

Foams are dispersed systems and can only be generated when both the gaseous (dispersed) and aqueous (continuous) phases are present in the pore space, with a sufficient water fraction and concentration of foaming agent. Different injection strategies have been proposed to fulfil these requirements. Continuous foam injection, where the aqueous and gaseous phases are co-injected, is rarely used in the field (Rossen, 1995), due to operational constraints and potential injectivity issues. The most used foam injection process is Surfactant-Alternating-Gas (SAG) that mitigates the reduced injectivity expected during co-injection by generating a weaker foam near the injection well (Rossen et al., 1995), in addition to decreasing gravity override (Shan and Rossen, 2004; Shi and Rossen, 1998). When gravity-driven segregated flow occurs, interaction between the surfactant (foaming agent, aqueous phase) and gas will be limited because the phases are flowing in separate zones of the reservoir, observed by Vassenden et al. (1999) at the semi-reservoir scale.

Two modified foam injection processes have been proposed, where CO_2 soluble surfactants are dissolved in the gaseous phase to act as the foaming agent, Water-Alternating-Gas-with-Surfactant-in-Gas (WASG), and continuous Surfactant-Gas injection (SG) (Le et al., 2008). Use of CO_2 soluble surfactants may improve the utilization of the foaming agent. Foam and surfactant transport simulations during WASG by Zeng et al. (2016) concluded that the distribution of surfactant throughout the reservoir was improved when the surfactant partitions equally between the gaseous and aqueous phases (i.e. the surfactant had a partitioning coefficient of unity). Foam strength is dependent on surfactant concentration (Jones et al., 2016). McLendon et al. (2014) and Xing et al. (2012) observed a higher foam strength when using partially CO_2 soluble surfactants dissolved in both injected phases (brine and CO_2), compared to foam floods where only one of the injected phases contained surfactant. The lower foam strength may be explained by a decreasing surfactant concentration within the pore space because partitioning occurs when surfactant is only present in one phase.

This paper investigates the effect of foam on the CO_2 storage capacity during unsteady state foam floods. Results from a laboratory evaluation of six commercially available surfactants, used to generate CO_2-foam at reservoir conditions are presented. Dense CO_2 was injected into a long sandstone core initially saturated by each surfactant to investigate foam generation and decay. The same sandstone core was used for all foam floods, thoroughly cleaned between each surfactant. Uncertainties associated with core material heterogeneity and varying experimental conditions were thus diminished. A model to estimate surfactant stripping was developed and expected surfactant stripping was compared with measured foam decay.

2. Methods and materials

2.1. Rock material

The unsteady state injections were performed in a cylindrical, outcrop Bentheimer sandstone core (Table 1). Porosity was determined by weight measurements, and the liquid absolute permeability was calculated using Darcy's law with three injection rates. A single core was used during all injections to eliminate the impact from changing core properties. The core was cleaned and re-saturated with surfactant before each CO_2 injection.

Table 1
Core properties.

Length (cm)	114.8 ± 0.01
Diameter (cm)	3.79 ± 0.01
Pore Volume (ml)	301.8 ± 0.5
Porosity	0.232
Permeability (Darcy)	± 0 .15

Table 2
Composition of synthetic seawater. All salts were EMSURE salts (Merck Millipore) supplied by VWR.

Component	Concentration [wt. %]
Deionized water	96.2
NaCl	2.31
$CaCl_2 \cdot 2H_2O$	0.19
$MgCl_2 \cdot 6H_2O$	0.90
KCl	0.07
Na_2SO_4	0.33

2.2. Fluid preparation

Synthetic seawater (brine) was prepared by dissolving salts into deionized water (Table 2) and filtered through a 0.45 µm cellulose acetate filter to remove possible large particles. Five commercially available non-ionic surfactants were purchased from Sigma-Aldrich and used as foaming agents (Table 3). A $C_{14\text{-}16}$ alpha olefin sulphonate (AOS) was kindly supplied by the Stepan Company and was used as a reference anionic surfactant. Measured CO_2 partitioning coefficients (kp), *i.e.* the distribution of the surfactant between CO_2 and brine at equilibrium were used to investigate this effect on foam behaviour. A constant surfactant concentration (0.5 wt. %) in synthetic seawater was used for all surfactant solutions. The surfactant solutions were flushed with Argon to remove dissolved oxygen and stored under an Argon atmosphere. CO_2 of 99.9999 % purity was used during foam injection.

The partitioning coefficients were measured using an internally stirred windowed variable volume pVT cell from D. B. Robinson (Barrabino et al., 2020). The surfactant concentrations were determined using HPLC (Beranger and Holt, 1986). The measurements of partitioning coefficient were performed using 0.5 wt. % surfactant solutions that constituted 25 % of the total system volume, thus CO_2 constituted 75 % (Fig. 1). This volume distribution is similar to foam flooding, where end point surfactant solution saturation ranged between 9.5–21.5 % pore volume (PV).

2.3. Experimental procedure

To reduce radial CO_2 diffusion the core was wrapped in a 0.025 mm thick nickel foil before instalment in the Viton rubber sleeve in the biaxial core holder (Fig. 2). Methanol was injected to increase pore pressure, fill pore space with a liquid and to calculate porosity by measuring the difference of methanol injected and produced (adjusted for system dead volumes). Methanol was miscible displaced by several

Table 3
Surfactants used as the foaming agents. Partitioning coefficient were measured at 40°C and 200 bar.

Commercial Name	Type	kp [wt. %/wt. %]
Anionic, not CO_2-soluable		
BIO-TERGE® AS-40 (AOS)	$C_{14\text{-}16}$ sodium olefin sulfonate	0
Non-ionic, partially CO_2-soluble		
Tergitol 15-S-9	Branched alkyl ethoxylate	1.45 ± 0.14
Tergitol TMN 10	Branched alkyl ethoxylate	0.87 ± 0.01
Tergitol NP 10	Branched alkylphenol ethoxylate	0.10 ± 0.00
Igepal CO 720	Linear nonylphenol ethoxylate	0.22 ± 0.00
Brij L23	Lauryl ethoxylate.	0.02 ± 0.00

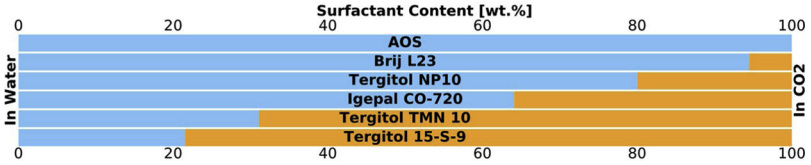

Fig. 1. The distribution of the surfactants between synthetic sea water (blue) and CO_2 (orange) at 40°C and 200 bar. AOS is not soluble in CO_2 and its content in CO_2 is therefore zero.

pore volumes of brine. The pore pressure was 200 bar and the overburden confinement pressure was 268 bar during injection of surfactant solutions and CO_2. The temperature in the heated zone was 40 °C when non-ionic surfactant solutions (CO_2-soluble surfactants) were injected and 80 °C when the anionic surfactant was used.

The core was fully saturated with surfactant solution when CO_2 was injected to investigate foam generation and decay. A gravity stabilized (top to bottom) CO_2 injection (as shown in Fig. 2) was used. The inline humidifier (placed upstream of the core) saturated the injected CO_2 with water vapour. Produced fluids were separated at atmospheric conditions, where the aqueous phase was collected in a graded cylinder and the produced CO_2 was vented through a two-column water adsorption unit (W. A. Hammond Drierite Comp. Ltd.). The combined mass of the produced liquids and vapour were logged on a balance, enabling calculation of the average water saturation in the core during CO_2 injections. The differential pressure across the core was logged versus time using three Fuji differential pressure transmitters of different pressure ranges (320 mbar, 5 bar and 20 bar), and reported as foam apparent viscosity μ_{app}.

$$\mu_{app} = \frac{k}{u} * \nabla p \tag{1}$$

In Eq. (1) k is the permeability, $\underline{u}$ is the Darcy velocity and ∇p is the pressure gradient.

The core temperature and inlet-, outlet-, back-pressure regulator and confinement pressures were also logged versus time during the experiments.

Two CO_2 injection schemes were used for each surfactant solution; the L-scheme and the H-scheme (Fig. 3). In the L-scheme, denoted *low* and abbreviated "L", a Darcy velocity of 2.1 ft/day (0.63 m/day) was applied during the initial part of the flooding; whereas a 32.5 ft/day (9.9 m/day) Darcy velocity, denoted *high* and abbreviated "H", was used during the initial part of the H-scheme. The injection rate was reduced within each scheme when the differential pressure and core saturation were converging towards stable conditions. For each surfactant one foam flood was performed for both injection schemes (L and H); thus, in total 12 unsteady state foam floods. The CO_2 injections with surfactant solution initially in the pore space were benchmarked against a run with brine (denoted baseline). The baseline was performed at 2.1 ft/day Darcy velocity.

The following procedure was used for all unsteady state CO_2 foam floods:

1) A minimum of 2.5 PV surfactant solution (min. 3773 mg of surfactant) was injected to satisfy surfactant adsorption, displace the brine and fully saturate the pore space with surfactant solution. Surfactant adsorption was measured in separate experiments.
2) *CO_2 was injected into the top of the vertically aligned core, using rates corresponding to either L-scheme or H-scheme injection (Fig. 3).
3) The core was cleaned by injecting solutions of 2-propanol and water and SSW (further described below), and finally re-saturated with brine.
4) Step 1) – 3) was repeated for all surfactant solutions.

2.4. Core cleaning

Surfactant solution and CO_2 was removed from the core and the flow lines between the foam floods by injection of water-based 2-propanol solutions and SSW. This involved injection of first a 2-propanol/water azeotrope (87.7 wt. % 2-propanol) followed by SSW. For some of the experiments a mixture of 0.5 wt.% NaCl with 30 wt.% 2-propanol was injected prior to SSW, and several injection cycles were done. The cleaning continued until no surfactant could be observed in the produced SSW and consistent water permeabilities were measured (2.91 ± 0.15) Darcy. The baseline CO_2 injection (no surfactant present) was performed between two of the foam injections. Foam generation was not observed during this experiment.

2.5. Surfactant mass model

A one-dimensional, piston-like displacement surfactant mass model was set up to estimate in-situ surfactant concentration and surfactant stripping during CO_2 injection. The saturation front advances one cell per time step with two possible water saturations: $S_w = S_{wr}$ behind the front and $S_w = 1$ ahead of the saturation front. S_{wr} is the residual water saturation after CO_2 flooding. The model assumes that both fluids are incompressible and that the surfactant distribution between the two phases is at local equilibrium. Surfactant adsorption and desorption at the rock-fluid interface are neglected. The total surfactant mass in a cell x at the time t ($m_s^{x,t}$) equals the sum of surfactant mass dissolved in CO_2 flowing from the upstream cell ($m_{CO_2}^{x-1,\,t-1}$) and the surfactant mass

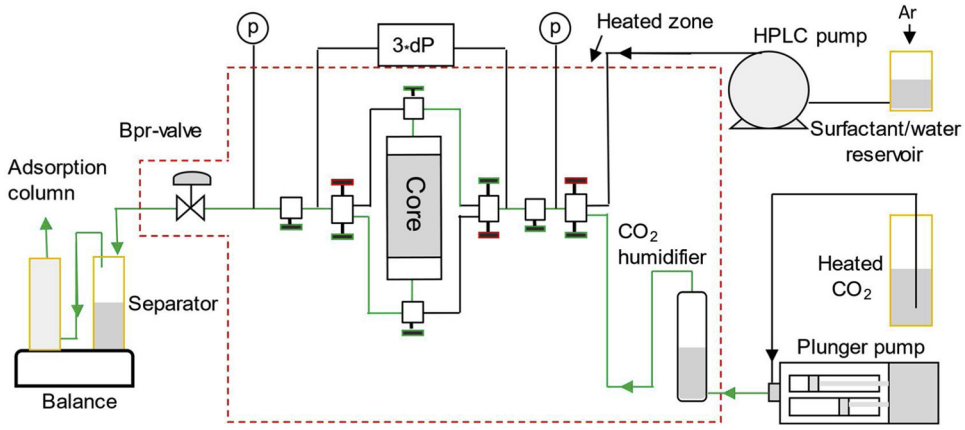

Fig. 2. Experimental setup used for the unsteady state foam experiments. Lines marked green indicates where fluids were flowing during CO_2 injection: Pure CO_2 from the Quizix Q5210 plunger pump was injected via the CO_2 humidifier and through a series of needle valves (marked green for open, red for closed) to the top of the core. Produced fluids from the bottom of the core was depressurized through the back-pressure regulator valve (BPR-valve) and collected in the separator and adsorption column placed on the balance. The HPLC pump was used to injected aqueous solutions (brine, surfactant solutions and cleaning fluids).

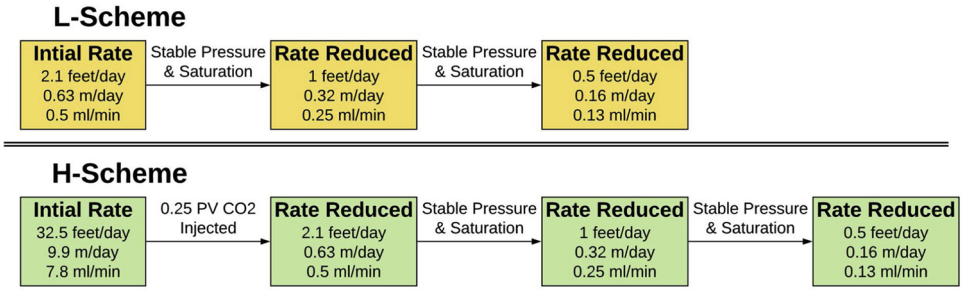

Fig. 3. L- and H- Injection schemes for foam floods. The injection rates are shown as Darcy velocities in field units ($feet/day$) or metric units (m/day) and as volumetric injection rates (ml/min). Criteria for rate change are included.

dissolved in the irreducible aqueous phase ($m_{s,W}^{x,t-1}$):

$$m_s^{x,t} = m_{s,CO_2}^{x-1,t-1} + m_{s,W}^{x,t-1} \tag{2}$$

The surfactant mass in residual water is assumed stagnant in the model, and the CO_2 flowing into the first cell does not contain surfactant.

Behind the saturation front, the surfactant partitions between both aqueous and gaseous phases. By assuming partitioning at local equilibrium, the relationship between the concentrations of surfactant in the two phases is given by the partitioning coefficient k_p, defined as:

$$k_p = \frac{\frac{m_{s,CO_2}}{m_{s,CO_2} + m_{CO_2}}}{\frac{m_{s,W}}{m_{s,W} + m_W}} \tag{3}$$

here m_{s,CO_2} and $m_{s,SW}$ are the masses of surfactant dissolved in the CO_2 and aqueous phase, and m_{CO_2} and m_W are the masses of CO_2 and aqueous phase, respectively. For low surfactant concentrations, the partitioning coefficient can be expressed as:

$$k_p = \frac{\frac{m_{s,CO_2}^{x,t}}{\rho_{CO_2}(1-S_W)}}{\frac{m_{s,W}^{x,t}}{(S_W)}} \tag{4}$$

where ρ_{CO_2} is the CO_2 density, the brine density is set to unity and the water saturation is S_W.

The mass of surfactant in each cell, $m_s^{x,t}$,is given by Eq. (2). The new distribution of surfactant can be calculated in water and CO_2 (at equilibrium) can be calculated by rewriting Eq. (4), giving:

$$m_{s,CO_2}^{x,t} = \frac{\frac{k_p * \rho_{CO_2}(1-S_W)}{S_W} * m_s^{x,t}}{\frac{k_p * \rho_{CO_2}(1-S_W)}{S_W} + 1} \tag{5}$$

The calculations were done for every individual cell (in total 100 cells) for each time step (0.01 PV). The total mass of surfactant present in the system, and in each phase, at a time t can be found by summarizing the individual surfactant mass of each cell.

3. Results

Experimental results from 13 core flooding experiments are given in the Fig. 4. The measured differential pressures recorded during the floods are converted to apparent viscosities using Eq. (1). The apparent viscosities versus pore volumes of CO_2 injected are plotted with a specific colour for each surfactant used consistently through the paper. The average water saturations are plotted using blue dashed lines. Reduction in rates are marked using yellow numbers (ml/min) and vertical lines. Data are available at http://doi.org/10.17632/4mp24c4jf7.1, an open-source online data repository hosted at Mendeley Data (Føyen and Holt, 2020).

Common observations for most of the floods seen in Fig. 4 are that the water saturation decreases linearly to low values (< 0.2) at breakthrough of CO_2. The linear decreases indicate that foam was generated and propagated with the same rate as the injected CO_2. Some experiments exhibited a different behaviour, however. For the H-Scheme injection with Tergitol 15-S-9 only weak foam was formed, resulting in non-piston like displacement with a early breakthrough of CO_2 production, and the low water saturation was obtained first after 1.5 PV injected CO_2. For the L-Scheme injection with Tergitol NP 10 CO_2 breakthrough occurred at 0.63 PV but strong foam was generated shortly after. The H-Scheme exhibited a similar but pronounced behaviour. CO2 breakthrough occurred at 0.69 PV. At 1.36 PV strong foam suddenly formed, and the water saturation quickly decreased to less than 0.2.

4. Discussion

4.1. Enhanced CO_2 storage using foam

The CO_2 storage capacity is here defined as the fraction of pore volume accessible for storing CO_2. The CO_2 storage capacity increased when foam was generated compared to baseline CO_2 injection without foam (Fig. 5). On average, the water saturation after 3 pore volumes of CO_2 injection ($S_{W,3PV}$) was 0.16 for the four surfactants that generated strong foam at the onset (foam generation characteristics discussed in detail below) compared to 0.34 for the baseline. Hence, the CO_2 storage capacity increased with 27 % when CO_2-foam was generated during CO_2 injection. A similar value was observed for CO_2 storage capacity at gas breakthrough (light blue) for most foam floods (except non-piston floods, marked by the red square **in** Fig. 5): The water saturation at breakthrough of CO_2, $S_{W,BT}$, was 0.21 with foam generation and 0.38 for the baseline; also a 27 % increase. The water saturation reduction observed during foam generation was attributed to increased microscopic water displacement (*i.e.* enhanced water mobilization at pore level) and can be considered as a secondary foam effect. The enhanced macroscopic sweep efficiency, the primary objective of foam injection, cannot be observed in a homogeneous sandstone core and downward injection.

A piston-like displacement of water was observed when foam was generated during CO_2 injection, with a sharp transition from water production to mainly gas production after gas breakthrough (Fig. 6). Water production continued after gas breakthrough, resulting in an additional CO_2 storage capacity of on average 6% for the foam floods (compared to 4% for the baseline).

Strong foam generation at the onset of CO_2 injection is beneficial for CO_2 storage, as the water saturation is reduced and, hence, the fraction of pore space occupied by CO_2 increases (Fig. 7). The difference between water saturations at gas breakthrough ($S_{W,BT}$) and end of injection ($S_{W,3PV}$) represents the efficiency of the CO_2-foam displacement process: a small difference indicates an efficient displacement of water and is preferable for optimizing CO_2 storage. In addition to foam generation, giving high pressure gradients, water saturation was possibly further reduced by reduced capillary forces as surfactants decrease the water/CO_2 interfacial tension (Lake et al., 2014). This becomes evident when comparing the baseline (no surfactant present, $S_{W,3PV} = 0.34$) to

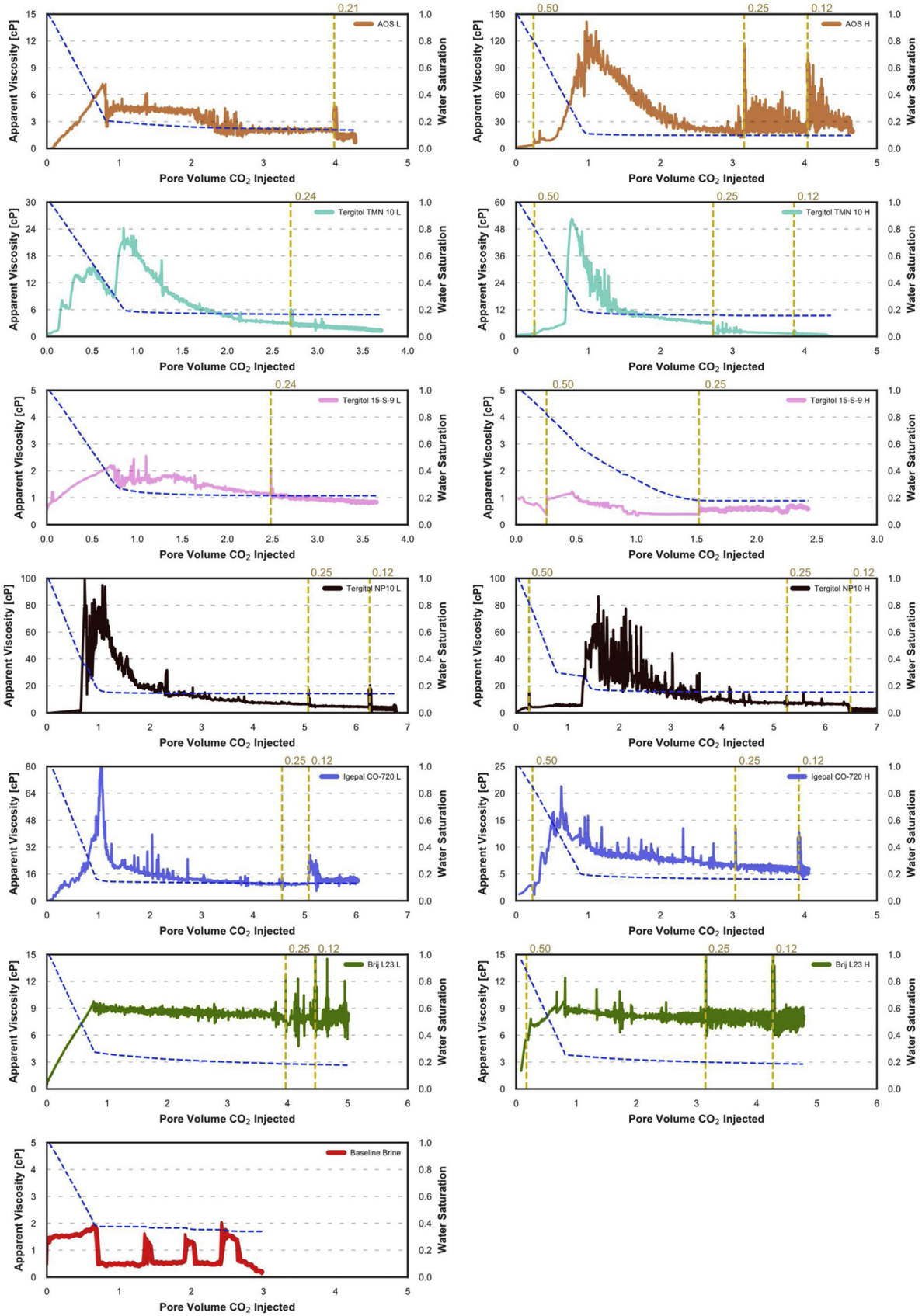

Fig. 4. Apparent viscosities (solid coloured lines) and water saturation (blue dashed lines) versus pore volumes of CO_2 injected for the foam and the baseline experiments. Left column L-scheme, right column H-scheme. Reduction in injection rate is shown using vertical yellow dashed lines, and the new rate (ml/min) is marked above.

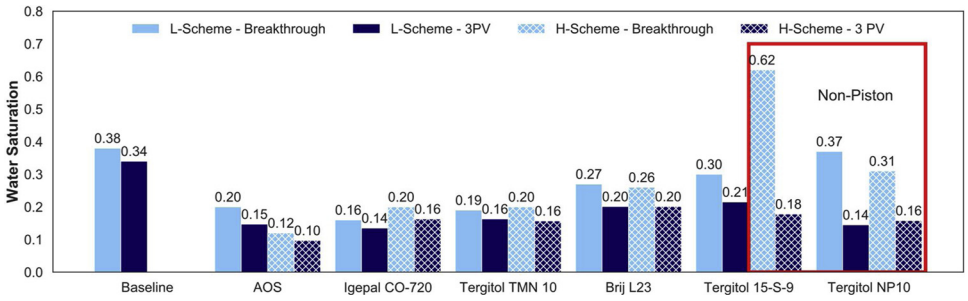

Fig. 5. Water saturations at gas breakthrough (light blue) and end of CO_2 injection (dark blue) using six commercial surfactants to generate CO_2-foam. Water saturations achieved with foam are compared to baseline CO_2 injection (no foam generated). Two CO_2 injection strategies were used: L-scheme (solid columns) and H-scheme (cross-hatched columns) for each of the six surfactants. Most CO_2-injections resulted in instant foam generation and a piston-like displacement of water, but three injections (H-scheme for Tergitol 15-S-9; L- and H-scheme for Tergitol NP10) exhibited non-piston displacement. The difference from piston-like and non-piston displacements (red rectangle) is discussed at length below.

Tergitol 15-S-9 (surfactant present, $S_{W,3PV} = 0.21$). The measured apparent viscosities for baseline and Tergitol 15-S-9 are similar (below 2 cP), but (L-scheme) end water saturations are different. Hence, the water displacement efficiency cannot be ascribed to increased differential pressures alone, but the interfacial tension reduction also contributes to low water saturations.

4.2. Onset foam generation

CO_2 foam generation, visualized by apparent viscosity calculated from differential pressure measurements (*cf.* Eq. (1)), occurred at the onset for most of the reported CO_2 injections. Foam apparent viscosity is expected to increase from the onset during unsteady state foam floods, when CO_2 advances through the core to generate foam and the viscous resistance increases. After CO_2 breakthrough the foam apparent viscosity is expected to decrease due to foam coalescence when the water saturation is reduced towards the critical saturation for the existence of foam (Vassenden and Holt, 2000), and for the CO_2 soluble surfactants; depletion of surfactant. The highest measured apparent viscosity (referred to here as *peak*) was therefore expected to be observed close to CO_2 breakthrough. Foam generation was further categorized based on the rate of apparent viscosity increase before CO_2 breakthrough:

Linear: constant foam strength behind the saturation front.

Super-linear: positive feedback by pressure gradients.

Linear apparent viscosity development demonstrates that foam is generated close to the piston-like saturation front and remained stable behind the front. The *super-linear* increase in apparent viscosity could occur due to positive feedback by pressure gradients, *i.e.* the strength of the foam depends on the pressure gradient, and the pressure gradient increases with increasing foam strength. Positive feedback is consistent with the observation of minimum pressure gradients for foam generation reported by Yu et al. (2018). The minimum pressure gradients may vary between foam systems and can be different for the surfactants described here. The AOS foam floods demonstrate both foam generation categories (Fig. 8); linear during the L-scheme foam flood and super-linear for the H-scheme. The initial short (0.25 PV injected) high injection rate period during the AOS H-scheme flooding caused a pressure gradient sufficient to generate foam 17 times stronger than what was measured during the AOS L-scheme flooding. The AOS surfactant had the highest foam strength ratio of all the surfactants tested (Table 4).

The gradient of increase in apparent viscosity was dependent on the flow velocity for the Brij L23 surfactant. The Brij L 23 H-scheme flood (Fig. 9) exhibited two separate linear gradients in increasing apparent viscosity; one prior to and one after rate reduction, of 42 and 7 cP/PV, respectively. At equal rate the H- and L-scheme linear gradients were comparable (7 cP/PV for the H-scheme and 11 cP/PV for the L-scheme). The foam generation category for both Brij L 23 foam floods was linear, although a higher gradient of increase in apparent viscosity was achieved during initial high rate injection (at a higher pressure gradient). The foam generated at the onset was, however, not strong enough to trigger a self-sustained feedback loop, hence the slope of apparent viscosity increase became close to the L-scheme at equal rates. Both Igepal CO-720 floods exhibited super-linear behaviour. The apparent viscosities for the two Tergitol 15-S-9 experiments were low, 2 cP for the L-scheme, and 1 cP for the H-scheme, which was only slightly larger than the baseline apparent viscosity (0.5 cP).

4.3. Delayed foam generation

The two Tergitol NP10 foam floods displayed delayed foam generation and did not follow the overall trend in Fig. 6. Delayed foam generation is defined here as an abrupt and rapid increase in apparent viscosity after an extended period of CO_2 injection where the foam generation was initially limited (less than 10 % of peak value). The development in apparent viscosity during delayed foam generation deviates from the linear or super-linear foam generation categories and the foam generation does not necessarily occur at the saturation front.

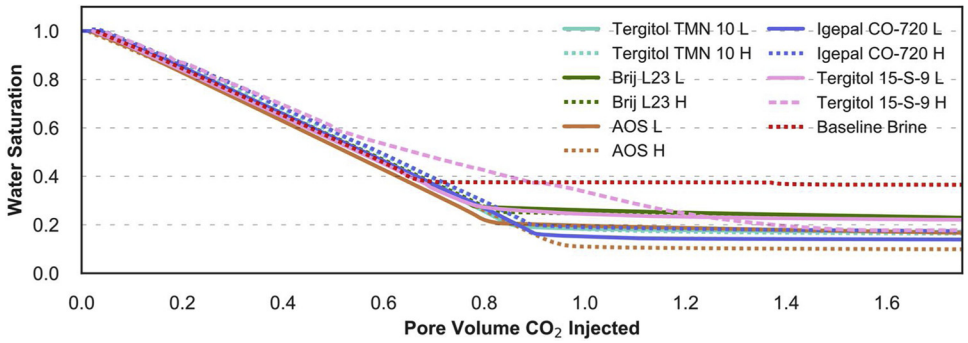

Fig. 6. Shows the water saturation versus pore volume CO_2 injected for the experiments behaving "piston-like". Tergitol 15-S-9 included to demonstrate a non-piston displacement with a non-linear reduction in water saturation when plotted against pore volumes CO_2 injected.

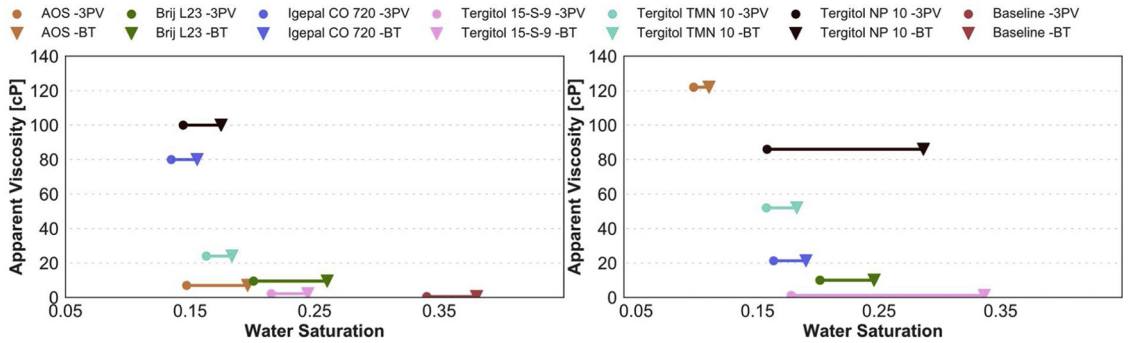

Fig. 7. Peak apparent viscosity versus water saturation at gas breakthrough (*Bt*, triangles) and after 3 PV of CO_2 injected (circles) during L-scheme (left) and H-scheme (right) for six commercial surfactants. Overall high peak apparent viscosities at breakthrough result in low water saturation and is beneficial for CO_2 storage capacity. The difference between water saturations at gas breakthrough and end of injection is indicated with a line between triangles and circles for each surfactant: short line represents an efficient displacement of water. Surfactants with delayed foam generation (Tergitol NP10 and 15-S-9) do not follow the overall trend as peak apparent viscosity occurs after gas breakthrough.

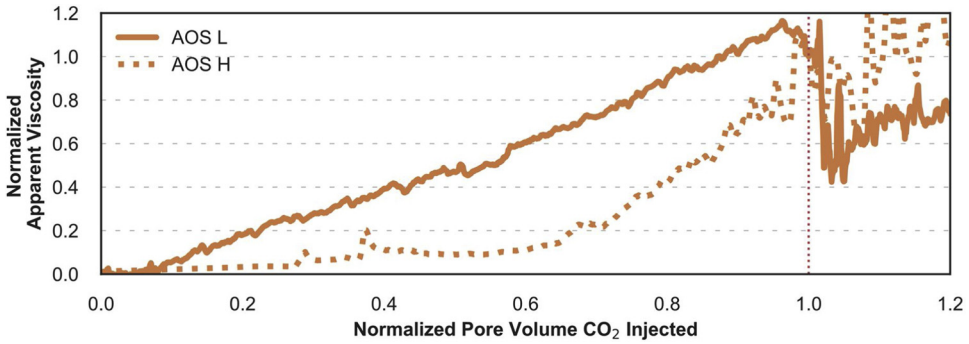

Fig. 8. Foam generation categories behaviours shown as development in apparent viscosity when CO_2 is injected exemplified by the two AOS foam floods: linear development (AOS L) and super-linear development (AOS H). Both apparent viscosity and pore volumes of CO_2 are normalized with respect to the values at gas break through.

Delayed generation of foam until gas breakthrough (Fig. 10: Tergitol NP 10, L-scheme) or later (Tergitol NP 10, H-scheme) caused an inefficient displacement of water, where the breakthrough saturation was closer to the baseline CO_2 injection. Additional storage of CO_2 was, however, achieved after foam generation due to a rapid increase in apparent viscosity and following stepwise mobilization of water. The Tergitol TMN 10 foam floods also displayed delayed foam generation, but foam generated before gas breakthrough (< 0.1 PV injected for L-scheme and 0.67 PV injected for the H-scheme) and efficient and linear reductions in water saturation were observed.

The mechanisms that determine whether foam generation occurs at the onset or is delayed are not clear. Reproducibility between all foam floods was ensured, because the same core was used, and the experimental conditions were equal and stable (except for the higher temperature used for the experiments with AOS). Variations in *e.g.* pore structure can therefore not explain the variation in foam generation behaviour. The reproducible conditions facilitate screening of surfactant (type and property) influence on foam generation- although this correlation is not straight forward. It is, however, interesting to observe that both surfactants generated foam within the same category during both L- and H-scheme floods (Table 5).

4.4. Foam decay

During unsteady-state foam floods, foam coalesce by reduction in water saturation and reduced surfactant concentration with increasing CO_2 saturation and throughput. Foam decay is identified here as consistently decreasing apparent viscosities after foam generation (Fig. 11). The CO_2 foam apparent viscosity decreased as more CO_2 was injected during L-scheme injections. The same trend was observed using the H-scheme but was less prominent. Tergitol NP 10 represents an obvious deviation from the trend due to delayed foam generation, and the low

Table 4
Foam generation categories for four surfactants used during unsteady state foam floods. The table includes the highest measured apparent viscosity for each foam flood (peak foam strength), when it was recorded (PV CO_2 injected at peak foam strength). The ratio between foam strengths during high (H) and low (L) rate foam floods are also given.

Foam flood:		Foam category	Peak foam strength:		Foam strength ratio [H/L]
Surfactant type	Injection Scheme		App visc. [cP]	Time [PV CO_2 inj.]	
AOS	L	Linear	7	0.77	17.4
	H	*Super-linear*	122	1.05	
Tergitol 15-S-9	L		2.2	0.71	0.56
	H		1.2	0.47	
Igepal CO-720	L	*Super-linear*	80	1.10	0.27
	H	*Super-linear*	21.3	0.60	
Brij L23	L	Linear	9.5	0.78	1.05
	H	Linear	10	0.80	
Baseline	L	–	0.5	–	

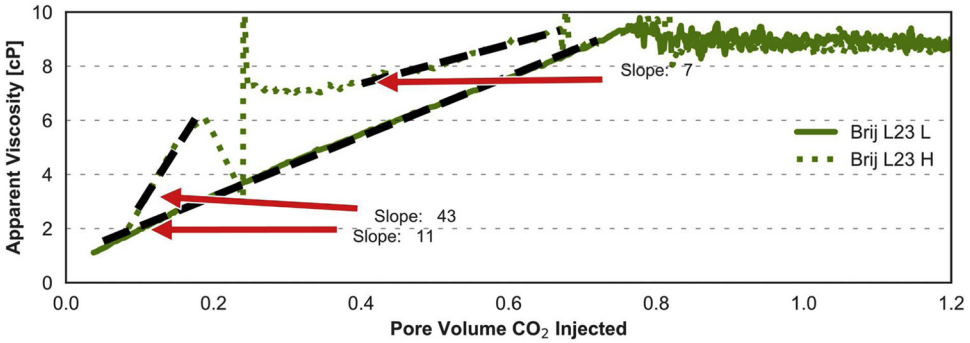

Fig. 9. Development in apparent viscosity (cP) during foam generation for the two Brij L23 experiments. The slopes of increase in apparent viscosity cP/PV are marked by dashed lines. The L-scheme had one distinct slope from the start of the experiment to gas breakthrough. The H-scheme had two distinct slopes; one prior to and one after rate reduction.

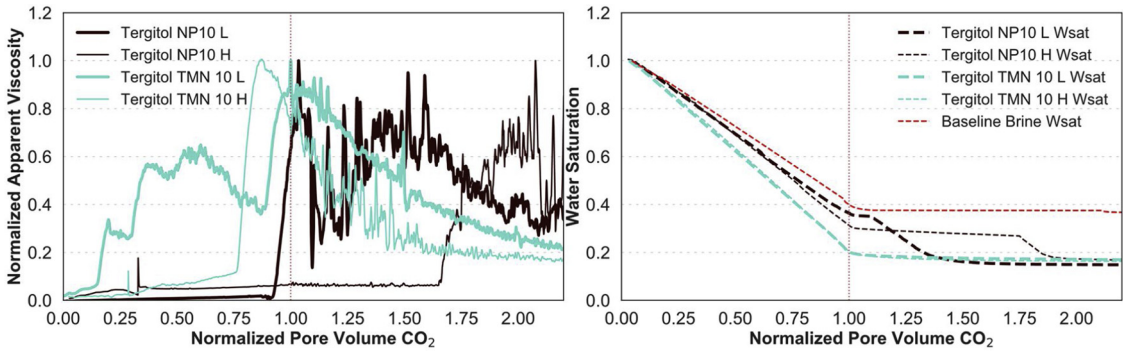

Fig. 10. Delayed foam generation was observed during CO_2 injection using surfactants Tergitol NP 10 and Tergitol TMN 10. The left figure shows apparent viscosity normalized to peak apparent viscosity, and the right figure shows water saturation development, both as functions of normalized time (PV CO_2 injected normalized to gas breakthrough). Gas breakthrough (1 PV) is indicated by the vertical red line. The water saturation profile for baseline CO_2 injection (no surfactant) is included for comparison.

Table 5
Foam generation categories for two surfactants used during unsteady state foam floods. The table includes the highest measured apparent viscosity for each foam flood (peak foam strength), when it was recorded (PV CO_2 injected at peak foam strength). The ratio between foam strengths during high (H) and low (L) rate foam floods are also given.

Foam flood:		Foam category	Peak foam strength:		Foam strength ratio [H/L]
Surfactant type	Injection Scheme		App visc [cP]	Time [PV CO2 inj]	
Tergitol TMN 10	L	Delayed	24	0.85	2.2
	H	Delayed	52	0.78	
Tergitol NP10	L	Delayed	100	0.75	0.86
	H	Delayed	86	1.60	
Baseline			0.5		

apparent viscosity observed when 1 PV CO_2 injected, resulting in foam coalescence to starting at 1.5 PV CO_2 for the H-scheme. Igepal CO-720 generated a weaker foam in the H-scheme CO_2 injection compared to the L-scheme, thus foam decay is more evident at low flow rates.

4.5. CO_2 solubility and surfactant stripping

Foam apparent viscosity depends on several factors, of which the surfactant concentration is vital (Jones et al., 2016). Surfactant stripping, where the surfactant concentration in the brine decreases due to partitioning into the CO_2, leads to reduced surfactant concentrations during unsteady state foam floods. This is of special interest when foam decay is considered. The surfactant mass balance model was used to calculate the concentration of non-ionic, partially CO_2-soluble surfactants in the core during CO_2 injection using experimentally measured partitioning coefficients (Fig. 12). The surfactant mass dissolved in CO_2 depends directly on the partitioning coefficient for each surfactant.

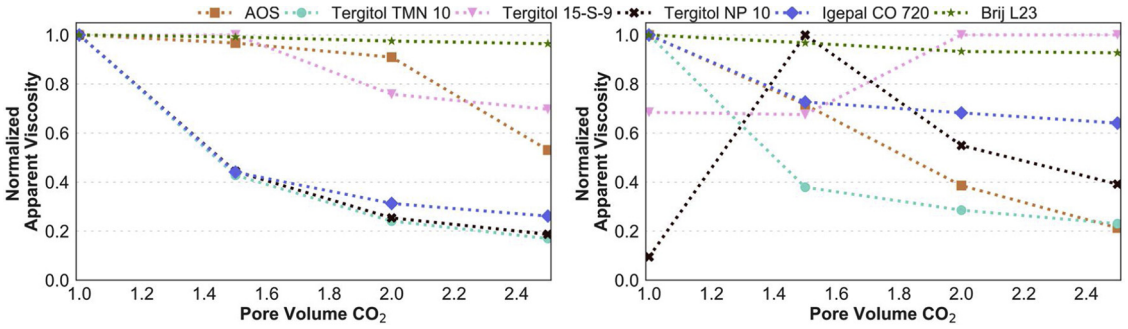

Fig. 11. Apparent viscosities plotted versus pore volumes of CO_2 injected using the L-scheme (left) and H-scheme (right). The apparent viscosities are normalized to the values measured at 1 PV injected for all experiments except Tergitol 15-S-9 H-scheme normalized at 2 PV injected and Tergitol NP10 H-scheme normalized at 1.5 PV injected.

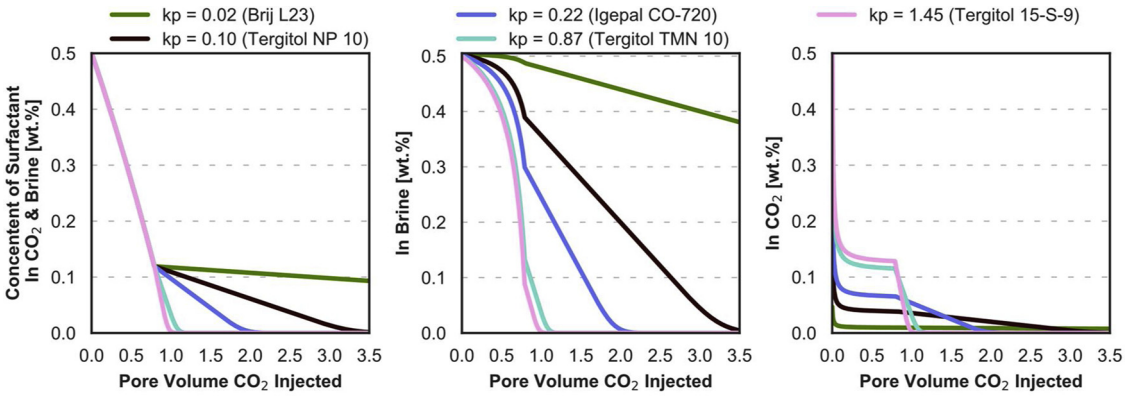

Fig. 12. Calculated total surfactant concentration (left) as a function of pore volumes CO_2 injected for different partitioning coefficient (kp). The partitioning coefficients used correspond to experimentally determined values for the five partially CO_2-soluble surfactants (see Table 3). The brand names are indicated for each kp. Surfactant concentrations in brine (middle) and CO_2 (right) are also shown. The residual water saturation was 0.2, and CO_2 density was 0.840 g/ml.

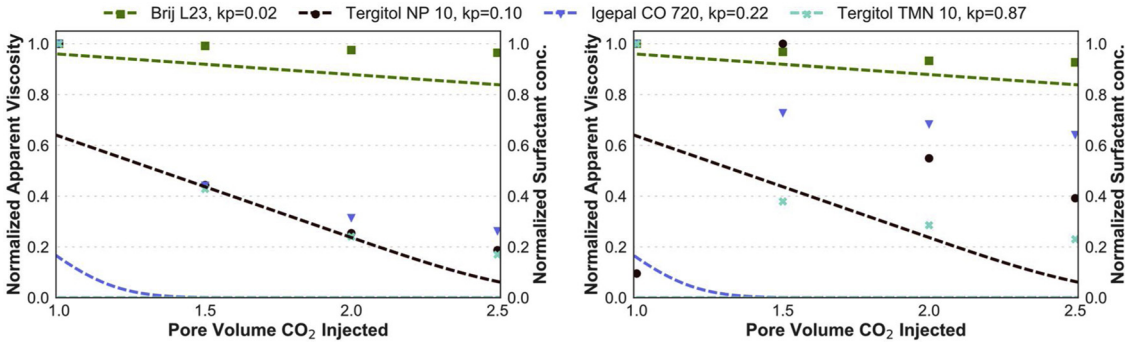

Fig. 13. Comparison between calculated surfactant concentrations using the surfactant mass balance model (dashed lines; normalized to concentration at CO_2 breakthrough) and measured apparent viscosity (points; normalized to the values measured at 1 PV injected for all experiments except Tergitol NP10 H-scheme normalized at 1.5 PV injected).

Before CO_2 breakthrough (at 0.8 PV CO_2 injected) the total surfactant concentration decreased linearly as surfactant-free CO_2 displaced the surfactant-rich brine in a piston-like manner. After CO_2 breakthrough the model assumes stagnant residual water, hence CO_2 is the only flowing phase. The model estimates a swift (low concentrations close to 1 PV injected) reduction in aqueous phase concentration due stripping of surfactants with high partitioning coefficients (kp > 0.22). Using a low (kp = 0.02) partitioning coefficient (Brij L23) resulted in a surfactant displacement that was nearly unaffected by stripping, and the total surfactant solution concentration remained almost constant after CO_2 breakthrough. In comparison, for high partitioning coefficients (Tergitol 15-S-9 and TMN 10) the total surfactant concentrations were essentially reduced to 0 after less than 1.25 pore volumes of CO_2 injected. Model results were compared with measured foam decay data (Fig. 13) using partitioning coefficients kp = 0.02 - 0.87, where foam decay is represented as normalized apparent viscosity. For surfactants not influenced by stripping (Brij L23) the model match experimental data well for both L- and H-scheme CO_2 injection. For the surfactants where surfactant stripping becomes important (high kp: Tergitol TMN10 and Igepal CO-720), the match is poor because the model estimates that surfactant concentrations reach 0 before 2 PV CO_2 injected whereas the measured apparent viscosities remained above 20 % of peak value after 2 PV CO_2 injected for both injection schemes.

Surfactant at the water-gas interface (*i.e.* lamellae) provides the lamella of self-healing capacity (Gibbs-Marangoni elasticity) which is the most important mechanism that stabilizes foam (Georgieva et al., 2009). The present model assumes local equilibrium for surfactant partitioning but does not account for surfactant adsorption on rock surfaces or at fluid interfaces. The kinetics of surfactant transport between the interfaces, the bulk fluids and the rock are not captured in the simplified model. Furthermore, adsorbed surfactant act as reservoirs of surfactant not included in the mass balance. Their magnitudes depend on the level of adsorption that can vary significantly depending on the type of surfactant. Additional complicating factors are that both the partitioning coefficients, the adsorption and foam strength depend on the surfactant concentration. The latter factor was observed for two of the present surfactants in steady state foam injection experiments (80 % foam quality, 200 bar and 40 °C) where the apparent viscosity measured for Igepal CO 720 at 0.013 wt.% surfactant was 12 % of the value measured for 0.5 wt. %. For Brij L23 the apparent viscosity measured at 0.010 wt.% surfactant was 71 % of the value measured for 0.5 wt. % (data not yet published).

All the simplifications inherent in the present model is demonstrated by results seen in Fig. 13. When the model predicts zero surfactant concentration in the core significant apparent viscosities are still observed. This show that surfactant was present in the core stabilising foam for several PVs of CO_2 injected after gas breakthrough.

The ability of surfactant to continue foam stabilization despite surfactant stripping can be beneficial during field scale application of CO_2 soluble surfactants, where the limited volume of injected surfactant (significantly less than one pore volume) can possibly be more efficiently utilized. Analyses using improved models that include the physical phenomena discussed above should be done in order to understand and reproduce the observed behaviour. This will also require additional laboratory data input such as the concentration dependence of the surfactant partitioning coefficients, surfactant adsorption/desorption isotherms and foam strength at variable surfactant concentrations. The kinetics of surfactant partitioning between fluids (the local equilibrium assumption) should also be studied. The kinetics can be important for laboratory time scale experiments but possibly less

important for reservoir scale behaviour.

5. Conclusions

CO_2-foam floods were stabilized by five non-ionic surfactants with varying degree of CO_2 solubility (partitioning coefficients) and one anionic surfactant insoluble in CO_2. The main observations during unsteady state foam floods were:

- All the tested surfactants generated foam, but the foam strength expressed as apparent viscosities varied depending on the surfactant used. For the anionic surfactant the initial injection rate of CO_2 affected the apparent viscosity significantly but had less impact for the non-ionic surfactants.
- Three categories of foam generation behaviour were observed. The build-up of foam in the core as function of the amount of CO_2 injected was characterised as linear, super-linear and delayed. The mechanism controlling foam generation category must be connected to the surfactant type and properties, as the core and experimental conditions were similar during 12 foam floods.
- Surfactant stripping into the flowing CO_2 caused continuous reductions in the surfactant concentration in the brine. This mass transfer was estimated using a simplified model. The observed foam decays were generally much slower than the estimated reductions in surfactant concentration. Surfactant adsorption on rock surfaces and at fluid interfaces were not included in the model. Adsorbed surfactant will act as reservoirs of surfactant depend on the level of adsorption. Additional complicating factors are that both the partitioning coefficients, the adsorption and foam strength depend on the surfactant concentration. A more detailed model of the physical phenomenon taking place is thus needed in order to fully understand the observed behaviours.
- Generation of foam combined with reduced water/CO_2 interfacial tensions during CO_2-foam floods yielded decreased residual water saturations compared to the baseline experiment without surfactant. This improvement in microscopic displacement comes in addition to the improved volumetric sweep expected by foam, implying increased storage capacity for sequestered CO_2.

Data availability

Datasets from the 13 core floods related to this article can be found at http://doi.org/10.17632/4mp24c4jf7.1, an open-source online data repository hosted at Mendeley Data (Føyen and Holt, 2020).ng.

CRediT authorship contribution statement

T. Føyen: Investigation, Formal analysis, Visualization, Writing - original draft. **B. Brattekås:** Writing - review & editing. **M.A. Fernø:** Writing - review & editing, Formal analysis. **A. Barrabino:** Investigation, Writing - review & editing. **T. Holt:** Project administration, Investigation, Writing - review & editing.

Declaration of Competing Interest

None.

Acknowledgements

Financial support from the Research Council of Norway is acknowledged for three ongoing projects: Improved performance of CO_2 EOR and underground storage by mobility control of CO_2 project no. 267859; Nanoparticles to Stabilize CO_2-foam for Efficient CCUS in Challenging Reservoirs project no. 268216; Subsurface Carbonate CO_2 Storage and Security project no. 280341; and for funding of PhD candidate Tore Føyen.

Appendix A. Supplementary data

Supplementary material related to this article can be found, in the online version, at doi:https://doi.org/10.1016/j.ijggc.2020.103016.

References

Alcorn, Z.P., Fredriksen, S.B., Sharma, M., Rognmo, A.U., Føyen, T.L., Fernø, M.A., Graue, A., 2019. An Integrated Carbon-Dioxide-Foam Enhanced-Oil-Recovery Pilot Program With Combined Carbon Capture, Utilization, and Storage in an Onshore Texas Heterogeneous Carbonate Field. Society of Petroleum Engineershttps://doi.org/10.2118/190204-PA.

Barrabino, A., Holt, T., Lindeberg, E., 2020. Partitioning of non-ionic surfactants between CO2 and brine. J. Pet. Sci. Eng. https://doi.org/10.1016/j.petrol.2020.107106.

Beranger, A., Holt, T., 1986. Middle and heavy α-olefin sulfonates. Tenside detergents 23, 247–254.

Bertin, H.J., Kovscek, A.R., 2003. Foam mobility in heterogeneous porous media. Transp. Porous Media 52, 17–35. https://doi.org/10.1023/A:1022312225868.

Cummings, S., Xing, D., Enick, R., Rogers, S., Heenan, R., Grillo, I., Eastoe, J., 2012. Design principles for supercritical CO2 viscosifiers. Soft Matter 8, 7044–7055. https://doi.org/10.1039/C2SM25735A.

Enick, R.M., Olsen, D.K., Ammer, J.R., Schuller, W., 2012. In: Mobility and Conformance Control for CO2 EOR via Thickeners, Foams, and Gels – A Literature Review of 40 Years of Research and Pilot Tests, SPE Improved Oil Recovery Symposium. Society of Petroleum Engineers, Tulsa, Oklahoma, USA. pp. 12. https://doi.org/10.2118/154122-MS.

Ettehadtavakkol, A., Lake, L.W., Bryant, S.L., 2014. CO2-EOR and storage design optimization. Int. J. Greenh. Gas Control. 25, 79–92. https://doi.org/10.1016/j.ijggc.2014.04.006.

Falls, A.H., Musters, J.J., Ratulowski, J., 1989. The Apparent Viscosity of Foams in Homogeneous Bead Packs. SPE-18069-PA 4. pp. 155–164. https://doi.org/10.2118/16048-PA.

Føyen, T., Holt, T., 2020. Core floods, increased CO2 storage capacity using CO2-foam, Mendeley Data. https://doi.org/10.17632/4mp24c4jf7.1.

Georgieva, D., Cagna, A., Langevin, D., 2009. Link between surface elasticity and foam stability. Soft Matter 5, 2063–2071. https://doi.org/10.2118/16048-PA.

Haugen, Å., Mani, N., Svenningsen, S., Brattekås, B., Graue, A., Ersland, G., Fernø, M.A., 2014. Miscible and immiscible foam injection for mobility control and EOR in fractured oil-wet carbonate rocks. Transp. Porous Media 104, 109–131. https://doi.org/10.1007/s11242-014-0323-6.

Hirasaki, G.J., Lawson, J.B., 1985. Mechanisms of Foam Flow in Porous Media: Apparent Viscosity in Smooth Capillaries. SPE-12129-PA 25. pp. 176–190. https://doi.org/10.2118/12129-PA.

IPCC, 2018. In: Masson-Delmotte, V., Zhai, P., Pörtner, H.-O., Roberts, D., Skea, J., Shukla, P.R., Pirani, A., Moufouma-Okia, W., Péan, C., Pidcock, R., Connors, S., Matthews, J.B.R., Chen, Y., Zhou, X., Gomis, M.I., Lonnoy, E., Maycock, T., Tignor, M., Waterfield, T. (Eds.), Summary for Policymakers, In: Global Warming If 1.5 C. An IPCC Special Report on the impacts of global warming of 1.5C above pre-industrial levels and related global greenhouse pathways, in the context of strengthening the global reponse to threat of climate change, sustainable development, and effort to eradicate poverty, Geneva, Switzerland, pp. 1–30.

Jones, S.A., Laskaris, G., Vincent-Bonnieu, S., Farajzadeh, R., Rossen, W.R., 2016. Effect of surfactant concentration on foam: From coreflood experiments to implicit-texture foam-model parameters. J. Ind. Eng. Chem. 37, 268–276. https://doi.org/10.1016/j.jiec.2016.03.041.

Lake, L.W., Johns, R.T., Rossen, R.W., Pope, G.A., 2014. Fundamentals of Enhanced Oil Recovery, second ed. Society of Petroleum Engineers, Richardson.

Lake, L.W., Lotfollahi, M., Bryant, S.L., 2019. Chapter 2 - CO2 enhanced oil recovery experience and its messages for CO2 storage. In: Newell, P., Ilgen, A.G. (Eds.), Science of Carbon Storage in Deep Saline Formations. Elsevier, pp. 15–31. https://doi.org/10.1016/B978-0-12-812752-0.00002-2.

Le, V.Q., Nguyen, Q.P., Sanders, A., 2008. A Novel Foam Concept With CO2 Dissolved Surfactants, SPE Symposium on Improved Oil Recovery. Society of Petroleum Engineers, Tulsa, Oklahoma, USA, pp. 15. https://doi.org/10.2118/113370-MS.

Lee, S., Kam, S.I., 2013. Chapter 2 - enhanced oil recovery by using CO2 foams: fundamentals and field applications. In: Sheng, J.J. (Ed.), Enhanced Oil Recovery Field Case Studies. Gulf Professional Publishing, Boston, pp. 23–61. https://doi.org/10.1016/B978-0-12-386545-8.00002-6.

Lee, J.J., Cummings, S., Dhuwe, A., Enick, R.M., Beckman, E.J., Perry, R., O'Brien, M., Doherty, M., 2014. In: Society of Petroleum Engineers, Tulsa, Oklahoma, USA. Development of Small Molecule CO2 Thickeners for EOR and Fracturing, SPE Improved Oil Recovery Symposium 18https://doi.org/10.2118/169039-MS.

Lindeberg, E., Grimstad, A.-A., Bergmo, P., Wessel-Berg, D., Torsæter, M., Holt, T., 2017. Large Scale Tertiary CO2 EOR in Mature Water Flooded Norwegian Oil Fields. Energy Procedia 114, 7096–7106. https://doi.org/10.1016/j.egypro.2017.03.1851.

McLendon, W.J., Koronaios, P., Enick, R.M., Biesmans, G., Salazar, L., Miller, A., Soong, Y., McLendon, T., Romanov, V., Crandall, D., 2014. Assessment of CO2-soluble non-ionic surfactants for mobility reduction using mobility measurements and CT imaging. J. Pet. Sci. Eng. 119, 196–209. https://doi.org/10.1016/j.petrol.2014.05.010.

Nguyen, P., Fadaei, H., Sinton, D., 2014. Pore-scale assessment of nanoparticle-stabilized CO2 foam for enhanced oil recovery. Energy Fuels 28, 6221–6227. https://doi.org/10.1021/ef5011995.

Rognmo, A.U., Horjen, H., Fernø, M.A., 2017. Nanotechnology for improved CO2 utilization in CCS: laboratory study of CO2-foam flow and silica nanoparticle retention in

porous media. Int. J. Greenh. Gas Control. 64, 113–118. https://doi.org/10.1016/j.ijggc.2017.07.010.
Rossen, W.R., 1995. Foams in Enhanced Oil Recovery, Foams: Theory: Measurements: Applications. Marcel Dekker, New York, pp. 413–464.
Rossen, W.R., Kibodeaux, K.R., Shi, J.X., Zeilinger, S.C., Lim, M.T., 1995. Injectivity and Gravity Override in Surfactant-Alternating-Gas Foam Processes, SPE Annual Technical Conference and Exhibition. Society of Petroleum Engineers, Dallas, Texas, pp. 12. https://doi.org/10.2118/30753-MS.
Shan, D., Rossen, W.R., 2004. Optimal Injection Strategies for Foam IOR. SPE-180051-PA 9. pp. 132–150.
Shi, J.X., Rossen, W.R., 1998. In: Improved Surfactant-Alternating-Gas Foam Process to Control Gravity Override, SPE/DOE Improved Oil Recovery Symposium. Society of Petroleum Engineers, Tulsa, Oklahoma. pp. 132–150. https://doi.org/10.2118/88811-PA.
Vassenden, F., Holt, T., 2000. Experimental Foundation for Relative Permeability Modeling of Foam. SPE-58047-PA 3. pp. 179–185. https://doi.org/10.2118/62506-PA.
Vassenden, F., Holt, T., Ghaderi, A., Solheim, A., 1999. Foam Propagation on Semi-Reservoir Scale. SPE-58047-PA 2. pp. 436–441. https://doi.org/10.2118/58047-PA.
Vitoonkijvanich, S., AlSofi, A.M., Blunt, M.J., 2015. Design of foam-assisted carbon dioxide storage in a North Sea aquifer using streamline-based simulation. Int. J. Greenh. Gas Control. 33, 113–121. https://doi.org/10.2118/58047-PA.
Xing, D., Wei, B., McLendon, W.J., Enick, R.M., McNulty, S., Trickett, K., Mohamed, A., Cummings, S., Eastoe, J., Rogers, S., Crandall, D., Tennant, B., McLendon, T., Romanov, V., Soong, Y., 2012. CO2-Soluble, Nonionic, Water-Soluble Surfactants that Stabilize CO2-in-Brine Foams. SPE-180051-PA 17. pp. 1172–1185. https://doi.org/10.2118/129907-PA.
Yu, G., Rossen, W.R., Vincent-Bonnieu, S., 2018. Foam Generation with Flow Rate: Effect of Surfactant Concentration and Gas Fraction, SPE EOR Conference at Oil and Gas West Asia. Society of Petroleum Engineers, Muscat, Oman, pp. 13. https://doi.org/10.2118/190398-MS.
Zeng, Y., Ma, K., Farajzadeh, R., Puerto, M., Biswal, S.L., Hirasaki, G.J., 2016. Effect of surfactant partitioning between gaseous phase and aqueous phase on CO2 foam transport for enhanced oil recovery. Transp. Porous Media 114, 777–793. https://doi.org/10.1007/s11242-016-0743-6.
Zhang, S., She, Y., Gu, Y., 2011. Evaluation of polymers as direct thickeners for CO2 enhanced oil recovery. J. Chem. Eng. Data 56, 1069–1079. https://doi.org/10.1021/je1010449.